Available online at www.sciencedirect.com
SCIENCE DIRECT®
PERGAMON
Control Engineering Practice 12 (2004) 31–40
CONTROL ENGINEERING PRACTICE
www.elsevier.com/locate/conengprac

Frequency adaptive control technique for rejecting periodic runout ☆

Jieng-Jang Liu, Yee-Pien Yang*

Department of Mechanical Engineering, National Taiwan University, No. 1, Roosevelt Road, Sec. 4, Taipei, Taiwan, 106, ROC

Received 8 April 2002; accepted 11 November 2002

Abstract

This paper proposes a novel adaptive controller for rejecting the periodic runout of a track-following system in the compact disk drive (CDD) with dual actuators. The control objective is to attenuate adaptively the specific frequency contents of runout disturbances without amplifying its rest harmonics. This controller can be implemented in a plug-in manner to an existing feedback control system without changing the original control setup. It is applicable to both the spindle modes of constant linear and constant angular velocity for various operation speeds. The experimental results show that the novel control strategy leads to a satisfactory performance in terms of the reduction of tracking error of CDDs.

Keywords: Compact disk drive; Runout rejection; Adaptive control; Track-following system

1. Introduction

Periodic disturbance occurs in various control engineering applications of the rotational mechanical systems. For compact disk drives (CDD), the spirally shaped tracks are usually not perfectly circular and the assembly of the disk and spindle motor is unavoidably eccentric. The resulting periodic disturbance is, therefore, synchronous with the disk rotation, and becomes particularly noticeable for the track-following servo system. These disturbances cause a large steady-state error at the frequencies of integer multiples of disk rotation. The conventional feedback regulation strategy usually did not consider these periodic disturbances; therefore no better asymptotical track-following can be achieved. For that reason, the runout components pose the perpetual tracking errors and degrade system performances.

According to the compact disk operation, there are various playing speeds of spindle modes of constant angular velocity (CAV) and constant linear velocity (CLV). Depending on the media types of stored data, the system processor selects a suitable running speed and spindle type for correct media playing. Between the two rotating types, the disk rotation is fixed at high speed for the CAV operation, while the speed is descent linearly for the CLV operation. Once the disk is running, the runout disturbances are present for both spindle modes, and the disturbance cancellation is necessary for better tracking performances.

The methods for eliminating periodic disturbances with fixed fundamental frequency were classified as four different repetitive control algorithms (Kempf, Messner, Tomizuka, & Horowitz, 1993). Among them, the adaptive repetitive controller (ARC) (Dötsch & Smakman, 1995) and adaptive feedforward cancellation (AFC) (Weerasooriya, Zhang, & Low, 1996; Onuki, Ishioka, & Yada, 1998; Lee, 1997) schemes were most widely used for disk drives; some analysis and synthesis methods were also reported (Bodson, Sacks, & Khosla, 1994; Sacks, Bodson & Messner, 1995; Messner & Bodson, 1994). These methods can be classified as the internal model principle (IMP) based controller design (Bodson et al., 1994). For the typical AFC method, the coefficients were continuously estimated and adapted for the on-line description of the sinusoidal disturbance. Experimental results reported in Weerasooriya et al. (1996), Lee (1997) and Sacks, Bodson and Messner (1995) verified that the modified AFC method was efficiently implemented on the disk drive, while the improved works dedicated by Sacks, Bodson and Messner (1995) and Messner and Bodson (1994) showed

☆ This research is accomplished by the aid of financial supports from the National Science Council of Taiwan, Republic of China, under Contract No. NSC90-2213-E002-083.

*Corresponding author. Fax: +886-2-23631755.
E-mail address: ypyang@ccms.ntu.edu.tw (Y.-P. Yang).

0967-0661/03/$ - see front matter © 2003 Elsevier Science Ltd. All rights reserved.
PII: S0967-0661(02)00283-6

various schemes to improve the robustness and performance of the AFC. In addition, depending on the available adaptation method used in AFC design, the work (Bayard, 1997) formulated the necessary and sufficient conditions for the AFC controller design. However, it is shown by Sacks, Bodson and Messner (1995) that, an AFC algorithm designed to cancel a specific harmonic could attenuate or amplify the rest ones as well. Furthermore, as shown by Kempf et al. (1993), the necessary requirement of the plug-in repetitive controllers was that the sampling time had to be adjusted so that an integer number of samples, N, matched the period of the fundamental frequency. In this regard, the implementation of AFC is limited to the disk operation at a CAV. For optical disk drives, however, variable rotating speeds with two spindle types make such implementation of their proposed repetitive controllers impossible.

In order to deal with the repeatable runout cancellation for both the CAV and CLV spindle modes in the optical disk drive, a novel frequency adaptive control technique (FACT) is proposed. The new frequency adaptive controller design depends only on the disk position, thereby independent of the spindle type and playing speed of the disk. Indeed, the new development of the on-line calculation method involves the creation of a frequency sampling filter (FSF) bank, by which the individual components of the runout disturbance can be extracted. This figure of merits leads to the result that the rejection of specific components of runout harmonics will not influence the rest ones. Therefore, the proposed method becomes suitable for both the spindle modes of CAV and CLV without changing the control setup. Implemented with the original feedback controller, the novel frequency adaptive controller is realized by a fixed-point FPGA to validate its application for a CDD.

In the proceeding sections, a brief description of the CDD is depicted in Section 2. The frequency adaptive control mechanism is introduced in Section 3, where the frequency sampling filtering and the adaptation algorithm are elaborated. Next, the proposed frequency adaptive controller is implemented with a CD-ROM drive, and the experiments are performed in Section 4 . Experimental results show that the proposed controller has successfully rejected the undesired harmonics of the runout disturbance to reach a satisfactory tracking performance. Final section summarizes the conclusions.

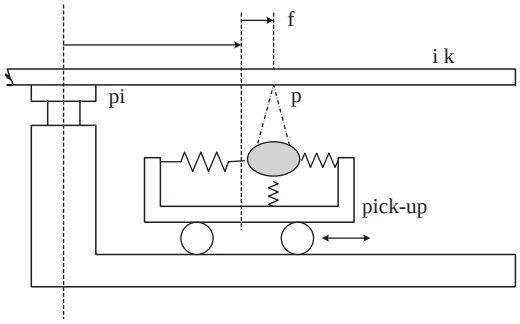

Fig. 1. Optical disk mechanism.

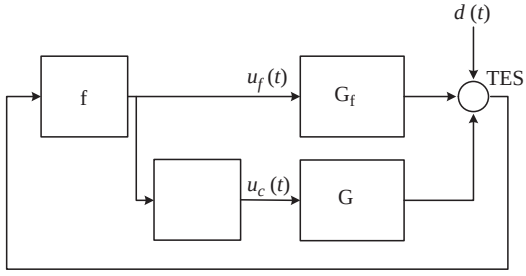

Fig. 2. Conventional MISO servo system.

2. The conventional servo system of CDD

The schematic diagram of a typical optical disk system is shown in Fig. 1. The mechanism is composed of a spindle motor for the rotation of the disk, an optical pick-up head for focusing and track following, and a coarse actuator to move the pick-up assembly in radial direction. During the operation of track-following, the laser spot follows the track by two-dimensional actuators: a DC sled motor for coarse motion, and a voice coil motor for fine motion adjustment. These two actuators possess different dynamic characteristics. The fine actuator has faster response with a narrow displacement range, while the coarse actuator moves across the entire disk radius with lower bandwidth. The position x_f of the objective lens and x_c of the pick-up head determine the laser spot position, thereby forming a multi-input single-output servo system as shown in Fig. 2. The transfer functions of fine and coarse actuators are denoted as $G_f(s)$ and $G_c(s)$, while the variables $u_f(t)$ and $u_c(t)$ are the control inputs to $G_f(s)$ and $G_c(s)$, respectively. The feedback controller $C_f(s)$ and $C_c(s)$ are designed so that the closed-loop system is stable, rejecting the external disturbance $d(t)$ and reaching a tolerable level of tracking error. Without knowing the relative displacement between the pick-up and the fine actuator during the track-following phase, only measured is the tracking error signal $e(t)$, which is commonly abbreviated to TES.

3. Algorithm of FACT

The frequency adaptive control mechanism is realized in a common used plug-in configuration as shown in Fig. 3 (Ohmori, Narita, & Sano, 1998; Sutton & Elliott, 1995), in which the proposed algorithm of FACT is illustrated in Fig. 4. The plant $G_f(s)$ effected by the

periodic disturbance $d(t)$ is controlled by the controller $C_f(s)$ as well as the compensation $v(t)$ through the plug-in FACT. The FACT algorithm consists of a frequency sampling filter and a gradient descent algorithm. The former calculates the magnitude and phase of individual frequency component from the error signal $e(t)$ which is measured with a fixed number of samples at each period, while the later adapts the magnitude and phase of the control output to compensate the error signal. To achieve accurate track-following, the TES is first filtered by a low pass filter, and sampled at N equally spaced points for each complete rotation of the disk. Then, the complete frequency contents of $e(t)$ caused by the disturbance $d(t)$ are extracted through the FACT. During the disk operation, the FACT only requires the last N samples of the error signal for the on-line calculation of the magnitude and phase of its individual component. Theoretically, the higher the harmonic components to be rejected, the more are points to be sampled for each rotation of the disk. Elaborated in the following section are the bank of frequency sampling filters and the adaptation mechanism that constitute the FACT.

3.1. Frequency sampling filter

The frequency sampling filter (FSF) is a finite-impulse-response filter and is similar to the discrete Fourier transform used in the digital signal processing (Bitmead & Anderson, 1981). The impulse response of FSF can be completely described by the N points equally spaced around the unit circle; the corresponding frequency contents are extracted through a bank of transfer functions as follows:

$$H_n(z) = \frac{1 - z^{-N}}{1 - W_N^n z^{-1}} = 1 + W_N^n z^{-1} + W_N^{2n} z^{-2} + \cdots + W_N^{n(N-1)} z^{-(N-1)}, \tag{1}$$

where $W_N^n = \exp(j(2\pi n/N))$ and $n = 0, 1, \ldots, N-1$. The input and the output of the nth elemental filter of the FSF bank are denoted by $e(k)$ and $\xi_n(k)$, respectively, and a batch of N samples of $e(t)$ per period is needed for each filtering process, as shown in Fig. 5. Since the elemental filter $H_n(z)$ has $N-1$ zeros at points $z = W_N^i$ for $i \neq n$ on the unit circle, only the magnitude and phase of the nth harmonics of the specific periodic signal are identified. Therefore, this bank of $H_n(z)$ produces a collection of spectral components, which approximate the frequency contents of the input periodic signal.

Theorem 1. *Let the periodic signal $e(t)$ be given by the sinusoidal functions with fundamental frequency ω_1, i.e.,*

$$e(t) = \sum_{n=1}^{M} (a_n \cos \omega_n t + b_n \sin \omega_n t), \tag{2}$$

where M is the highest harmonic order, $\omega_n = n\omega_1$, and a_n and b_n are unknown variables indicating the in-phase and quadrature of individual harmonic component. Then,

(I) *the output of each elementary FSF for input $e(t)$, which is sampled at N equally spaced points, is described as $\xi_n(k)$,*

$$\xi_n(k) = H_n(z)e(k) = \frac{N}{2}(\alpha_n + j\beta_n), \tag{3}$$

where

$$\begin{cases} \alpha_n = a_n \cos \omega_n t + b_n \sin \omega_n t, \\ \beta_n = a_n \sin \omega_n t - b_n \cos \omega_n t, \end{cases} \tag{4}$$

$n = 1, 2, \ldots, M$, *and the least value of N is*

$$N = 2M + 2, \tag{5}$$

(II) *the parameters a_n and b_n in (2) are obtained by the coordinate transformation*

$$\begin{cases} a_n = \alpha_n \cos \omega_n t + \beta_n \sin \omega_n t, \\ b_n = \alpha_n \sin \omega_n t - \beta_n \cos \omega_n t. \end{cases} \tag{6}$$

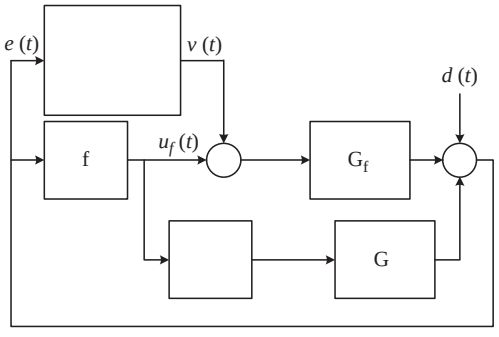

Fig. 3. The plug-in configuration of frequency adapting control.

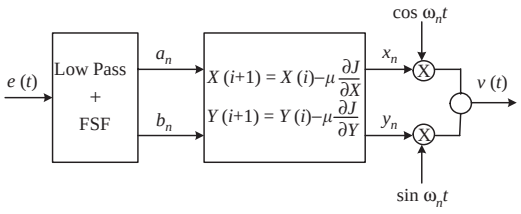

Fig. 4. The block representation of the algorithm of FACT.

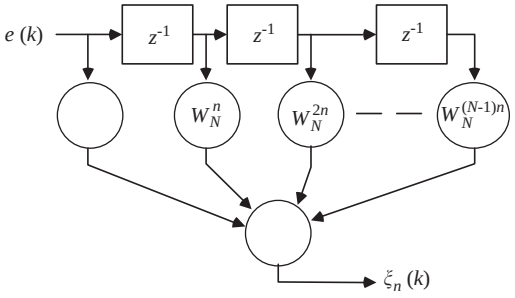

Fig. 5. One elemental FSF realization.

Proof. The proof is delineated in the appendix.

From Theorem 1, the parameters a_n and b_n describing the measured periodic signal $e(t)$ in (2) are calculated on-line by the bank of FSF defined in (1). It is also worth noticing that not a full bank of FSF filters but only the first M elementary filters is needed for FSF algorithm to be implemented.

3.2. Adaptation formulation

The runout disturbance $d(t)$ is periodic and causes the measured tracking error $e(t)$ with the same frequency. As shown in Fig. 3, the transfer function from $v(t)$ to the tracking error $e(t)$ of the plant is expressed as

$$\frac{e}{v} = \frac{G_f}{1 + G_f C_f + G_c C_c C_f}. \tag{7}$$

Since the bandwidth of the coarse actuator is much smaller than the runout frequencies, only the fine actuator is implemented with the FACT algorithm to reject the runout effects. This leads to the transfer of reduced order as

$$\frac{e}{v} = \frac{G_f}{1 + G_f C_f} = W(s). \tag{8}$$

The addition of FACT output $v(t)$ to the input $u_f(t)$ results in a compensated control input, TRO, to the fine actuator $G_f(s)$. The control objective aims at canceling the runout effect asymptotically by the compensation of $v(t)$. In terms of the first M harmonics of $e(t)$, the adaptation signal $v(t)$ is defined as

$$v(t) = \sum_{n=1}^{M} (x_n \cos \omega_n t + y_n \sin \omega_n t), \tag{9}$$

where, the on-line adaptation of variables x_n and y_n are to be formulated. The following adapting mechanism is modified from, and more efficient than, the work by Sutton and Elliott (1995).

Let vectors $\mathbf{A}$, $\mathbf{B}$, $\mathbf{X}$ and $\mathbf{Y}$ be $\mathbf{A} = [a_1\ a_2 \cdots a_M]^{\mathrm{T}}$, $\mathbf{B} = [b_1\ b_2 \cdots b_M]^{\mathrm{T}}$, $\mathbf{X} = [x_1\ x_2 \cdots x_M]^{\mathrm{T}}$, $\mathbf{Y} = [y_1\ y_2 \cdots y_M]^{\mathrm{T}}$, where, a_n and b_n are given by (6) and x_n and y_n are variables described in (9). The penalty function for the adaptation is defined as the total energy of the measured error at each harmonic frequencies ω_n such that

$$J = \tfrac{1}{2}(\mathbf{A}^{\mathrm{T}}\mathbf{A} + \mathbf{B}^{\mathrm{T}}\mathbf{B}). \tag{10}$$

The gradient descent algorithms are described in terms of x_n and y_n as

$$\begin{cases} \mathbf{X}(i+1) = \mathbf{X}(i) - \mu \dfrac{\partial J}{\partial \mathbf{X}}, \\ \mathbf{Y}(i+1) = \mathbf{Y}(i) - \mu \dfrac{\partial J}{\partial \mathbf{Y}}, \end{cases} \tag{11}$$

where, the adaptation gain μ is positive such that the descendent of J is guaranteed. The gradients of the penalty function J with respect to the vectors $\mathbf{X}$ and $\mathbf{Y}$ are written as

$$\frac{\partial J}{\partial \mathbf{X}} = \Phi_{ax}\mathbf{A} + \Phi_{bx}\mathbf{B},$$

$$\frac{\partial J}{\partial \mathbf{Y}} = \Phi_{ay}\mathbf{A} + \Phi_{by}\mathbf{B}. \tag{12}$$

By the definition, the Jacobean matrices Φ_{ij} in (12) are diagonal with constant coefficients, and represent the rate of change of the elements of $\mathbf{A}$ and $\mathbf{B}$ with respect to $\mathbf{X}$ and $\mathbf{Y}$, respectively.

Since the vectors $\mathbf{A}$ and $\mathbf{B}$ are updated on-line by the FSF described in Theorem 1, if the Jacobean matrices in (12) are known, this adaptation algorithm can be used to adjust the value of $v(t)$ such that the measured error $e(t)$ is minimized. It is clear that the response of the linear system $W(s)$ at a specific frequency depends only on the excitation of the same frequency. Therefore, the frequency response of $W(s)$ excited by the sinusoidal input of frequency ω_n is denoted by $[W_r(\omega_n) + jW_i(\omega_n)]$, and the input–output relationship becomes

$$a_n + jb_n = \{W_r(\omega_n) + jW_i(\omega_n)\}(x_n + jy_n), \tag{13}$$

where, $W_r(\omega_n)$ and $W_i(\omega_n)$ are, respectively, the real and imaginary parts of the frequency response of $W(s)$ at ω_n. Differentiating (13) with respect to x_n and y_n yields

$$\frac{\partial a_n}{\partial x_n} = W_r(\omega_n), \quad \frac{\partial a_n}{\partial y_n} = -W_i(\omega_n),$$

$$\frac{\partial b_n}{\partial x_n} = W_i(\omega_n), \quad \frac{\partial b_n}{\partial y_n} = W_r(\omega_n). \tag{14}$$

Hence, the combination of (11)–(14) constitutes an adaptation law as follows:

$$\begin{cases} x_n(i+1) = x_n(i) - \mu[W_r(\omega_n)a_n + W_i(\omega_n)b_n], \\ y_n(i+1) = y_n(i) - \mu[-W_i(\omega_n)a_n + W_r(\omega_n)b_n] \end{cases} \tag{15}$$

with $n = 1, 2, \ldots, M$. It is worth noting that only the frequency responses at ω_n of system $W(s)$ are required to formulate the proposed adaptation law.

4. Implementation of FACT

4.1. Experimental setup

The compact disk used in the experiment is a commercial high-speed CD-ROM drive. The drive functions properly with the original control structure, including spindle, focus, track following and track seeking servos. In order to validate the FACT, only the track following servo is rebuilt in the experimental setup as shown in Fig. 6. The TES is sampled at 175 kHz by an 8-bit A/D converter; frequency generator (FG) accounting for the disk position decoder signal has 6 logic outputs of square form in one revolution; tracking output (TRO) represents the fine actuator output driven

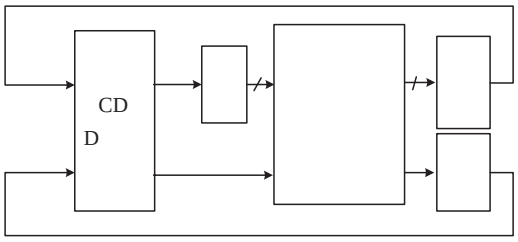

Fig. 6. Experimental setup.

by an 8-bit D/A converter; and feed motor output (FMO) is the output of the coarse actuator driven by a PWM power module. A single ALTERA EPF10KA FPGA device (ALTERA, 2002) is used to implement the track following controllers $C_f(s)$ and $C_c(s)$ as well as the proposed FACT algorithms. The FPGA is a programmable logic device. The ALTERA provides powerful logic design tools to fulfill the user's requirements. The implementation of FACT function as well as the controllers can be realized through the design environment of MAX-Plus II provided by ALTERA.

4.2. Experimental results

In this section, experimental results for the track-following mechanism implemented with the proposed FACT are described under the disk operating at variable high-speed CAV mode and the slow CLV mode. The proposed controller successfully rejects the runout disturbance and promotes better track following quality.

4.2.1. Constant angular velocity mode at 75 Hz

In the first experiment of the track-following control, the disk operates at the CAV mode of 75 Hz (4500 rpm). The corresponding frequency response $W(s)$ at frequencies between 10 and 1 kHz is obtained as shown in Fig. 7. The real and imaginary parts of the first four harmonic frequencies at 75, 150, 225 and 300 Hz are listed in Table 1. The real time TES under the conventional feedback control is shown in Fig. 8, where ch1 presents the time series of TES over three disk revolutions and ch2 presents its power spectrum through fast Fourier transformation (FFT), in which one voltage time response stands for 0.02 mm runout. The power spectrum of the TES shows that the runout error occurs at the integer multiples of the fundamental frequency, i.e., 75, 150, 225, 300, 375 Hz, etc. It is clear that the first four harmonics are dominant. In this case, the FACT is designed to cancel the first four harmonics, i.e. $M = 4$, and the least number of equally spaced sampling points of one revolution of the disk is $N = 2 \times 4 + 2 = 10$ as formulated in (5). When the fourth-order FACT is added to the system by means of the plug-in manner, the power spectrums of the TES are shown as illustrated in Fig. 9 under various conditions of runout rejection.

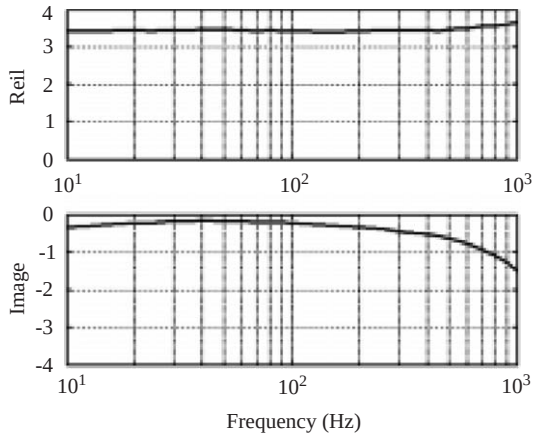

Fig. 7. Frequency response of $W(s)$ for disk running at CAV 75 Hz.

Table 1
The frequency response of $W(\omega_n)$

CAV mode at 75 Hz			CAV mode at Hz		
	ea	mae		ea	mae
ω	ω	ω	ω	ω	ω
75					
5				5	
5	5			5	
	5		5		57

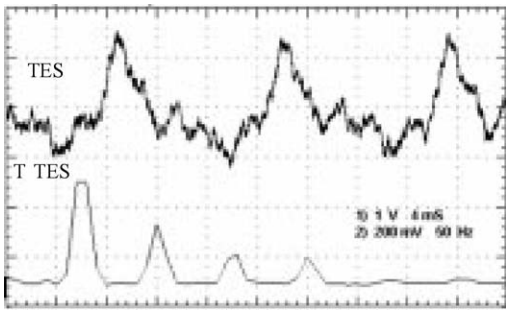

Fig. 8. The TES (ch1) and its FFT waveforms (ch2) for disk running at 75 Hz when the FACT turned off.

These four lines illuminate the corresponding FFTs of the compensated TES for the first through fourth bank of FACT, respectively. Compared to the ch2 in Fig. 8, it is evident that the FACT rejects the target frequencies without attenuating or amplifying other harmonics. Furthermore, when these four banks of FACT are added to the system simultaneously, as shown in Fig. 10, the first four harmonics of the tracking error are cancelled completely.

In view of the stability, it is important to examine whether the stability margins would be affected by the compensation of the FACT. Regardless of the runout disturbance $d(t)$, the sensitivity function

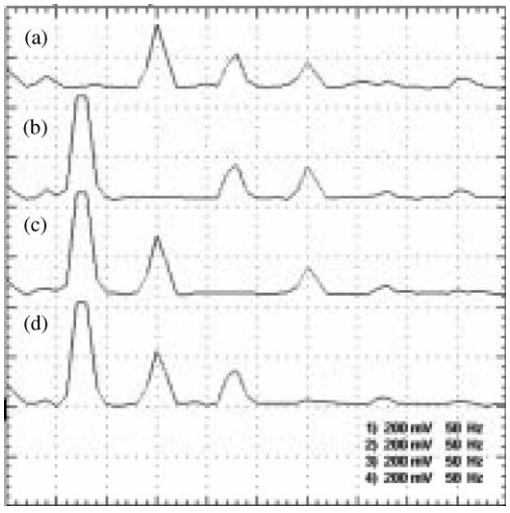

Fig. 9. The individual component cancellation of the FACT. The uncompensated components will neither be enlarged nor reduced. Plots (a)–(d) are the 1st, 2nd, 3rd and 4th harmonics been cancelled, respectively.

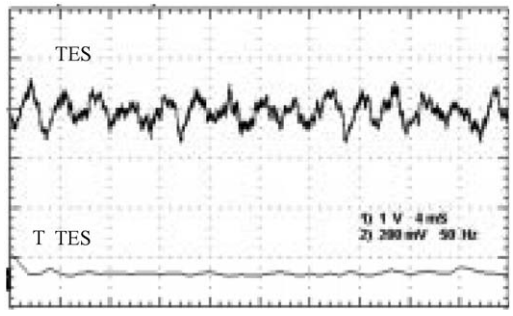

Fig. 10. The TES and its FFT waveforms after four banks of FACT turned on.

$S(s)$ and the complementary sensitivity function $T(s)$ can be defined as

$$S = \frac{\tilde{e}}{\rho} = \frac{1}{1 + G_f C_f}, \tag{16}$$

$$T = \frac{e}{\rho} = \frac{G_f C_f}{1 + G_f C_f}. \tag{17}$$

They are identified by the synchronized sinusoidal excitation $\rho(t)$ shown in the measuring setup Fig. 11. Since the runout disturbances $d(t)$ exist during the identification process, the relationship among $\tilde{e}(t)$, $\rho(t)$ and $d(t)$ is described by

$$\tilde{e} = \frac{1}{1 + G_f C_f}(\rho - d), \tag{18}$$

where the measurement of $\tilde{e}(t)$ is always contaminated by the runout disturbance $d(t)$ with significant contents at the frequencies of 75, 150, 225, 300 Hz, etc. This implies that the identification of (16) becomes impossible. Alternatively, defining the approximate sensitivity function as

$$S_a = \tilde{e}/\rho \tag{19}$$

then $S_a(s)$ is the same as $S(s)$ for all frequencies except at those harmonics and is extracted experimentally by measuring the gain and phase between output $\tilde{e}(t)$ and sinusoidal input $\rho(t)$ sweeping from 40 to 4 kHz. Figs. 12 and 13 show the frequency responses of $S_a(s)$ before and after the FACT function were added on, respectively. Without the FACT in Fig. 12, there are significant peak values at the first four harmonic frequencies, which arise from the disturbance $d(t)$ at

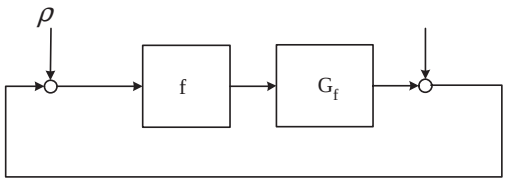

Fig. 11. The identification measuring setup for track-following system.

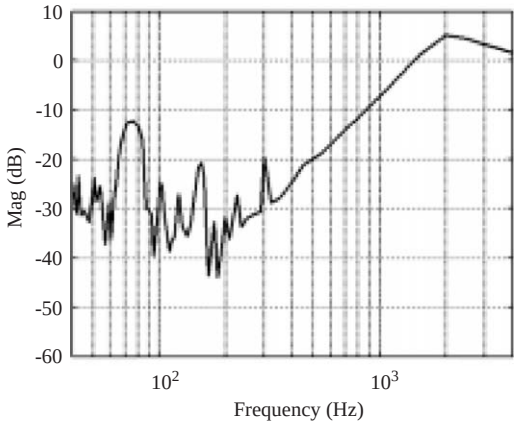

Fig. 12. The magnitude of $S_a(s)$ for disk running at CAV 75 Hz without the FACT.

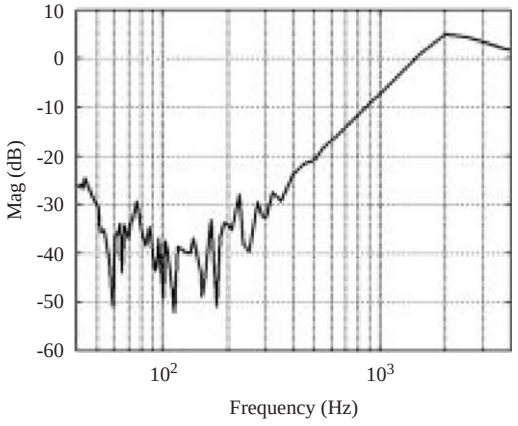

Fig. 13. The magnitude of $S_a(s)$ after the four banks of FACT turned on.

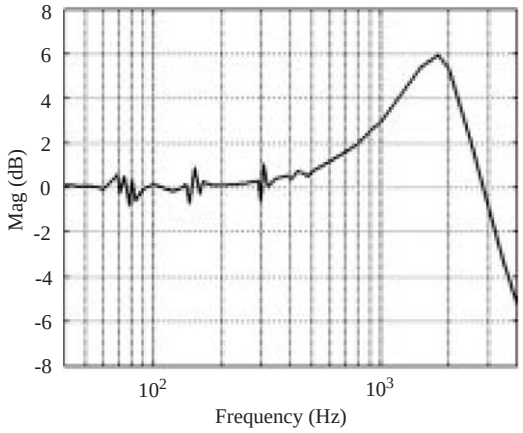

Fig. 14. The magnitude of $T_a(s)$ for disk running at CAV 75 Hz without the FACT.

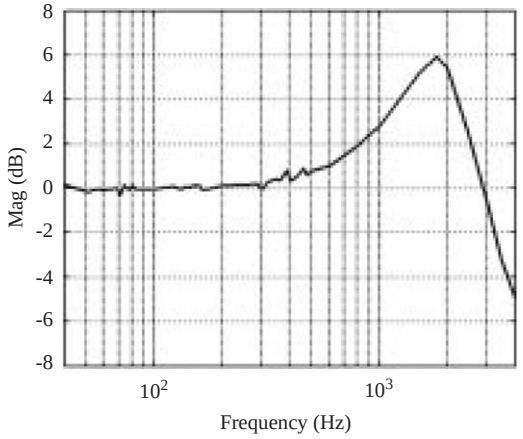

Fig. 15. The magnitude of $T_a(s)$ when the FACT were turned on.

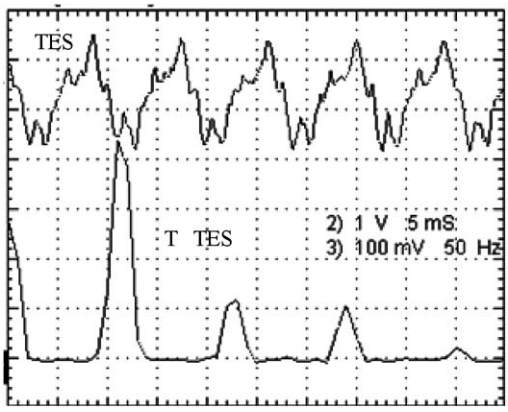

Fig. 16. The TES and its FFT waveforms for disk running at 113 Hz when FACT turned off.

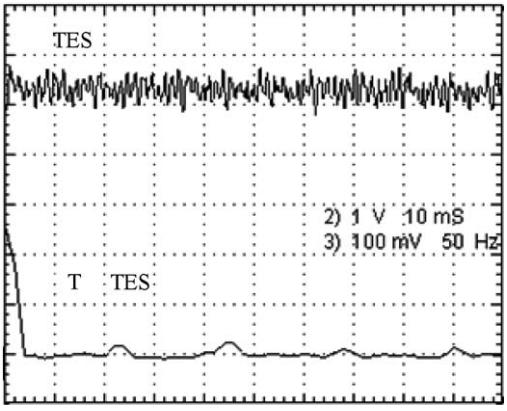

Fig. 17. The TES and its FFT waveforms for disk running at 113 Hz after FACT turned on.

their harmonic frequencies as depicted in (18). This leads to the result that the system has poor steady-state performance at these frequencies. It is clear that, as shown in Fig. 13, the FACT provides a mechanism causing the magnitude of $S_a(s)$ small at low frequencies, which is desired for good tracking and disturbance rejection. Hence, the stability margins at the frequencies of the first four harmonics have been extended, thereby achieving better system stability. Similarly, the approximate complementary sensitivity function $T_a = e/\rho$ is also contaminated by the runout disturbance $d(t)$, and can be identified without and with the FACT as shown, respectively, in Figs. 14 and 15. The FACT makes the magnitude of $T_a(s)$ close to unity at the first four harmonic frequencies, while the roll off behavior at high frequencies is reserved for high-frequency noise rejection.

4.2.2. Variable play speed verification

When the disk is speed up to 113 Hz (6780 rpm), the first four harmonic components become 113, 226, 339 and 452 Hz; and the corresponding frequency responses of $W(s)$ are also listed in Table 1. Figs. 16 and 17 show the time series and power spectrum of TES, before and after, respectively, the four banks of FACT are turned on. It is clear that the FACT works properly through a new set of coefficients of $W(\omega_n)$ at an alternative disk speed.

More experiments are done on the disk running at slower CLV modes. As used on the CAV mode, the FACT can be also implemented without changing the original control structure. Since the disk speed varies for different tacking ranges at the CLV mode, the values of $W_r(\omega_n)$ and $W_i(\omega_n)$ in (15) must change accordingly. Fortunately, these two variables have little change in low-frequency range as indicated in Fig. 7. That leads to the choice of a set of mean values of these two variables over a specific disk speed range at CLV mode to fulfill the FACT satisfactorily. Figs. 18 and 19 show the experimental results for the CLV case. The former presents the uncompensated TES signal and its power spectrum, while the latter reveals

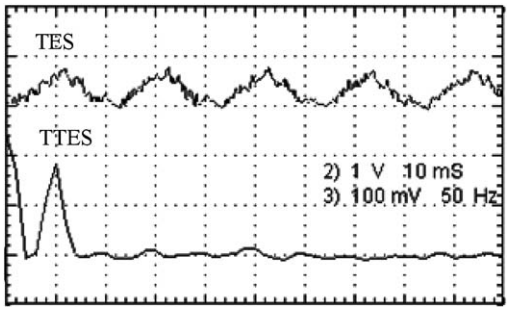

Fig. 18. The TES and its FFT waveforms for disk running at CLV when FACT turned off.

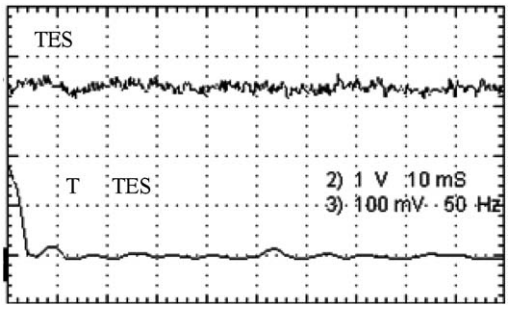

Fig. 19. The TES and its FFT waveforms for disk running at CLV after FACT turned on.

satisfactory runout rejection by the FACT. It is apparent that the dominant fundamental harmonic has been cancelled completely.

4.3. The settling properties of FACT

Indeed, the CD-ROM drives operate between the track-following and track-seeking one after another. At the end of seeking, the track-following proceeds immediately to read data from the target track. Therefore, the settling ability at the beginning of track-following becomes another requirement for runout rejection. The proposed FACT algorithm provides not only an efficient mechanism to cancel the runout effect during the track-following operation, but also a simple switching setup to fulfill the connection to the track-seeking phase. According to the block diagram of the FACT in Fig. 4, the adapting function in (15) can be turned off temporarily during the seeking operation. The last adapted values of x_n and y_n generate the compensated output $v(t)$ during the track-seeking, resulting in the lens moving in phase of the disk runout. For instance, a short outward seeking is examined for 10 tracks at a CAV mode of 113 Hz to show the suitable settling performance of the FACT. In Fig. 20, there is a steady and significant tracking error before and after the seeking operation for the feedback track-following without FACT. An acceptable settling behavior at the

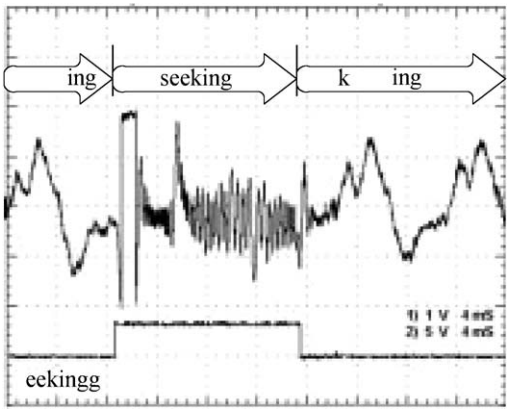

Fig. 20. The settling property between track-following and seeking operation in the original system without the FACT.

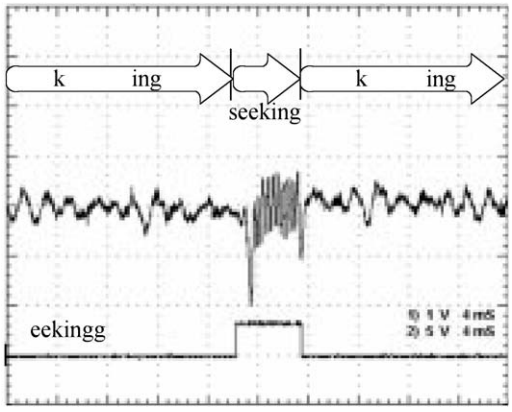

Fig. 21. The settling property with the FACT added on. The fast settling process could be reserved without the settle-out penalty.

transient period of the track-following may be obtained through well designed feedback controllers and the velocity profile used in the seeking operation. Having the FACT added on, the tracking error can be reduced significantly before and after the seeking period as shown in Fig. 21. It is clear that the fast settling process during the track pull-in phase is reserved and the runout rejection is fulfilled immediately as soon as the controller switched from the seeking operation.

By contrast with the method raised by Sri-Jayantha, Dang, Yoneda, Kitazaki, and Yamnmoto (2001), a settle-out penalty was used at the transient period of the track-following for suppressing the disk runout. However, the proposed FACT has the merit of compensating the disk runout all the way through seeking and track-following operations with continuously adapted control parameters. Once the compensation parameters x_n and y_n are initially tuned and converged during the first track-following mode, they are remained during the following track seeking operation; and the fine tuning proceeds at each start of the track-following, while no additional penalty is needed for the reduction of

tracking error. That way, the convergence rate is not critical and the control performance will not be changed between the switching of the track-following and seeking operation.

5. Conclusion

A novel frequency adaptive control technique is proposed and examined on a CDD. Both the theoretical and experimental results show that the periodic runout harmonics can be rejected simultaneously and efficiently for both CAV and CLV spindle modes under variable playing speed. The rejection devoted to some candidate harmonic components will not influence the uncompensated ones. In view of application requirement, the proposed FACT can be extended for the runout rejection to various compact disk drives, such as CD-ROM, CD-RW or DVD-ROM drives.

Appendix A. Proof of the Theorem 1

Let

$$W_N^n = \exp\left(j\frac{2\pi}{N}n\right) = \cos\theta_n + j\sin\theta_n,$$

where $\theta_n = 2\pi n/N$ and $n = 0, 1, \ldots, N-1$. Since the FSF has $N-1$ zeros at $z = W_N^i$ for $i \neq n$, the output of the nth elementary FSF for input $e(t)$ given by (2) is the same as the output driven by the nth input component

$$e_n(t) = a_n \cos\omega_n t + b_n \sin\omega_n t. \tag{20}$$

Once the input $e(t)$ has been sampled, its nth component can be denoted by

$$e_n(k) = a_n \cos k\theta_n + b_n \sin k\theta_n. \tag{21}$$

Thus,

$$\begin{aligned}\xi_n(k) &= H_n(k)e(k)\\ &= e(k) + W_N^n e(k-1) + W_N^{2n} e(k-2)\\ &\quad + \cdots + W_N^{(N-1)n} e(k-N+1)\\ &= \sum_{i=0}^{N-1} (\cos i\theta_n + j\sin i\theta_n)(a_n \cos(k-i)\theta_n\\ &\quad + b_n \sin(k-i)\theta_n)\\ &= 2\sum_{i=0}^{N/2-1} (\cos i\theta_n + j\sin i\theta_n)(a_n \cos(k-i)\theta_n\\ &\quad + b_n \sin(k-i)\theta_n),\end{aligned} \tag{22}$$

where the following properties of trigonometric functions applies:

$$\cos(N+i)\theta_n = \cos i\theta_n, \quad \sin(N+i)\theta_n = \sin i\theta_n,$$

$$\cos\left(\frac{N}{2}+i\right)\theta_n = (-1)^n \cos i\theta_n,$$

$$\sin\left(\frac{N}{2}+i\right)\theta_n = (-1)^n \sin i\theta_n.$$

For any $k \geqslant N$, summing up all the real and imaginary parts of (22) yields

$$\begin{aligned}\xi_n(k) = \frac{N}{2}[&(a_n \cos k\theta_n + b_n \sin k\theta_n)\\ &+ j(a_n \sin k\theta_n - b_n \cos k\theta_n)].\end{aligned} \tag{23}$$

Hence, Eqs. (3) and (4) follow. Furthermore, elementary trigonometric function properties

$$\cos\theta_{n+N/2} = -\cos\theta_n, \quad \sin\theta_{n+N/2} = -\sin\theta_n$$

implies

$$\xi_{n+N/2} = -\xi_n \tag{24}$$

which reveals that only $N/2$ outputs for the bank of FSF are independent. It follows that the least value of N is $N = 2 \times M + 2$ for the maximum order M. Finally, the transformation from (4) to (6) is straightforward by the transforming matrix

$$\Delta = \begin{bmatrix} \cos\omega t & \sin\omega t \\ \sin\omega t & -\cos\omega t \end{bmatrix}.$$

References

ALTERA (2002). *FLEX 10K embedded programmable logic family data sheet*. Altera Corporation. San Jose, CA, USA.

Bayard, D. S. (1997). Necessary and sufficient conditions for LTI representations of adaptive systems with sinusoidal regressors. *Proceedings of the American control conference*, New Mexico (pp. 1642–1646).

Bitmead, R. R., & Anderson, B. D. O. (1981). Adaptive frequency sampling filters. *IEEE Transactions on Acoustics, Speech and Signal Processing*, *Assp-29*(3), 684–693.

Bodson, M., Sacks, A., & Khosla, P. (1994). Harmonic generation in adaptive feedforward cancellation schemes. *IEEE Transactions on Magnetics*, *39*(9), 1939–1944.

Dötsch, H. G. M., & Smakman, H. T. (1995). Adaptive repetitive control of a compact disk mechanism. *Procceedings of the 34th conference on decision & control*, New Orleans (pp. 1720–1725).

Kempf, C., Messner, W., Tomizuka, M., & Horowitz, R. (1993). Comparison of four dicrete-time repetitive control algorithms. *IEEE Control Systems Magazine*, *13*(6), 48–54.

Lee, H. S. (1997). Implementation of adaptive feedforward cancellation algorithm for pre-embossed rigid magnetic (PERM) disks. *IEEE Transactions on Magnetics*, *33*(3), 2419–2423.

Messner, W., & Bodson, M. (1994). Design of adaptive feedforward controllers using internal model equivalence. *Proceedings of the American control conference*, Maryland (pp. 1619–1623).

Ohmori, H., Narita, N., & Sano, A. (1998). Plug-in adaptive controller for periodic disturbance rejection. *Proceedings of the 37th IEEE conference on decision and control*, Florida, USA (pp. 4529–4530).

Onuki, Y., Ishioka, H., & Yada, H. (1998). Repeatable runout compensation for disk drives using multi-loop adaptive feedforward cancellation. *Proceedings of the SICE annual conference*, Chiba (pp. 29–31).

Sacks, A. H., Bodson, M., & Messner, W. (1995). Advanced methods for repeatable runout compensation. *IEEE Transactions on Magnetics*, *31*(2), 1031–1036.

Sri-Jayantha, S. M., Dang, H., Yoneda, I., Kitazaki, N., & Yamnmoto, S. (2001). TrueTrack servo technology for high TPI disk drives. *IEEE Transactions on Magnetics*, *37*(2), 871–876.

Sutton, T. J., & Elliott, S. J. (1995). Active attenuation of periodic vibration in nonlinear systems using an adaptive harmonic controller. *Journal of Vibration and Acoustics*, *117*, 355–362.

Weerasooriya, S., Zhang, J. L., & Low, T. S. (1996). Efficient implementation of adaptive feedforward runout cancellation in a disk drive. *IEEE Transactions on Magnetics*, *32*(5), 3920–3923.